Cerebral Cortex, October 2021;31: 4794–4807

https://doi.org/10.1093/cercor/bhab123
Advance Access Publication Date: 20 May 2021
Original Article

ORIGINAL ARTICLE

Morphological Development Trajectory and Structural Covariance Network of the Human Fetal Cortical Plate during the Early Second Trimester

Feifei Xu[1,2,3,†], Mengting Liu[3,†], Sharon Y. Kim[3], Xinting Ge[1,3], Zhonghe Zhang[1,4], Yuchun Tang[1,2], Xiangtao Lin[1,4], Arthur W. Toga[3], Shuwei Liu[1,2] and Hosung Kim[3]

[1]Department of Anatomy and Neurobiology, Research Center for Sectional and Imaging Anatomy, Shandong Key Laboratory of Mental Disorders, Shandong Key Laboratory of Digital Human and Clinical Anatomy, School of Basic Medical Sciences, Cheeloo College of Medicine, Shandong University, Jinan 250012, Shandong, China, [2]Institute of Brain and Brain-Inspired Science, Shandong University, Jinan 250012, Shandong, China, [3]Laboratory of Neuro Imaging (LONI), USC Steven Neuroimaging and Informatics Institute, Keck School of Medicine of University of Southern California, Los Angeles, CA 90033, USA and [4]Department of Medical Imaging, Shandong Provincial Hospital, Shandong University, Jinan 250021, Shandong, China

Address correspondence to Shuwei Liu. Email: liusw@sdu.edu.cn

[†]Feifei Xu and Mengting Liu contributed equally to this work

Abstract

During the early second trimester, the cortical plate, or "the developing cortex", undergoes immensely complex and rapid development to complete its major complement of neurons. However, morphological development of the cortical plate and the precise patterning of brain structural covariance networks during this period remain unexplored. In this study, we used 7.0 T high-resolution magnetic resonance images of brain specimens ranging from 14 to 22 gestational weeks to manually segment the cortical plate. Thickness, area expansion, and curvature (i.e., folding) across the cortical plate regions were computed, and correlations of thickness values among different cortical plate regions were measured to analyze fetal cortico-cortical structural covariance throughout development of the early second trimester. The cortical plate displayed significant increases in thickness and expansions in area throughout all regions but changes of curvature in only certain major sulci. The topological architecture and network properties of fetal brain covariance presented immature and inefficient organizations with low degree of integration and high degree of segregation. Altogether, our results provide novel insight on the developmental patterning of cortical plate thickness and the developmental origin of brain network architecture throughout the early second trimester.

Key words: cortical plate, fetal brain development, high-resolution MRI, structural covariance network, thickness

© The Author(s) 2021. Published by Oxford University Press. All rights reserved. For permissions, please e-mail: journals.permissions@oup.com

Introduction

The developmental trajectory of the cerebral cortex is immensely complex yet highly organized. Starting around the eighth week of gestation, most neurons migrate from the ventricular and subventricular zones to the cortical plate along the radially oriented glial fiber (Rakic 1972, 2003; Sidman and Rakic 1973;). The neuronal migration activity peaks between 12 and 20 week of gestation (Gressens 2000; Webb et al. 2001). The cortical plate finishes its major complement of neurons cells by the end of gestational age 20–21 weeks (Bystron et al. 2008).

Following exuberant synaptogenesis, dendritic sprouting, and circuit formation, the cerebral wall of the second trimester exhibits typical fetal laminar organization (Rados et al. 2006; Kostovic and Vasung 2009). The marginal zone, the outermost layer of the cerebral wall, could be visualized as a high signal layer on high-resolution 7.0 T magnetic resonance imaging (MRI) (Zhang et al. 2011). The cortical plate is characterized by low T2-weighted (T2w) signal intensity due to the tight packing of cells. The subplate, a transient zone located beneath the cortical plate, is rich in extracellular matrix, and thus, appears hyperintense on T2w images (Rados et al. 2006). The immature cortical plate is the foundation for the future cerebral cortex, denoted as "the developing cortex" (Dubois et al. 2008). The second trimester of pregnancy, in particular, is a period of high vulnerability for fetuses, and relatively minor disruptions may significantly alter the structure and function of the mature brain and can pose long-term neurological consequences (Miranda 2012).

During the early second trimester, differences in gene expression in the developmental cortical plate regions were investigated using transcriptome analysis (Johnson et al. 2009; Kang et al. 2011). Diffusion tensor imaging (DTI) also revealed distinct fractional anisotropy (FA) values of cortical plate changes at different cortical areas between 13 and 21 weeks of gestation (Huang et al. 2013). The total thickness of the cortical plate and subplate were measured together (Huang et al. 2009). However, little is known about the morphological development of the cortical plate during this period.

Construction of the human brain network or connectome based on graph theoretical approaches opens new vistas on the early stages of brain development (Doria et al. 2010; Cao et al. 2017; Zhao et al. 2019). More specifically, structural covariance networks (SCNs) were used to characterize the inter-regional covariation patterns of gray matter morphology (e.g., volume, thickness, and surface area) across subjects (Zielinski et al. 2010; Geng et al. 2017; Scheinost et al. 2017). The nonrandom modular organization of covariance networks was observed in infants, possibly explaining reciprocal maturational signaling between two cortical regions that were connected. Furthermore, the segregation of the SCNs was reinforced from birth to 2 years of age (Fan et al. 2011; Nie et al. 2014). Differentially altered structural covariance among brain regions was discovered in prematurely born adolescents and young adults (Nosarti et al. 2011; Scheinost et al. 2017). During the fetal period, small world architecture and pronounced modular organization were observed at approximately 20 gestational weeks (GW) with diffusion MRI (Song et al. 2017) and functional MRI (Thomason et al. 2014). However, early configurations of developmental SCNs are not fully explored.

In clinical settings, in utero fetal MR scans can usually be acquired after 19 GW (Bendersky et al. 2008). On the other hand, because of difficulties associated with in utero imaging (e.g., fetal motion, presence of residual motion even after maternal breath-holding, complicated image processing for image reconstruction), the majority of existing connectome studies analyzed preterm infants mainly after 25 GW (Brown et al. 2014; Batalle et al. 2017). Postmortem fetal specimens provide an opportunity to study earlier brain development, which have advantages in obtaining high spatial resolution and high signal-to-noise ratio (SNR) images by allowing high-field-strength magnets, using a smaller field of view, reducing slice thickness, and increasing acquisition time.

In this study, using 7.0 T high-resolution MR images of fetal specimens between 14 to 22 GW, we first manually delineated the cortical plate and then calculated various morphological measurements including cortical thickness, sulcal depth, surface area, and mean curvature using a well-established surface-based framework. Furthermore, we constructed the SCN using the general linear model to explore early reciprocal cortico-cortical interaction of neurodevelopment. To the best of our knowledge and literature search, this is the first attempt to explore the development of cortical plate morphology and the fetal brain's SCN as early as 14 to 22 GW. Our results expand our understanding of the early developmental pattern of the cortical plate and can be used as a reference for future studies.

Materials and Methods

Materials

A total of 27 human fetal specimens of 14 to 22 GW were included in the current study, which were partially used in our previous fetal brain development studies of spatial–temporal atlas and hippocampal formation (Zhan et al. 2013; Ge et al. 2015). All postmortem fetuses were collected from hospitals in Shandong Province, China. A total of 16 specimens were obtained after medically indicated abortions caused by stressful intrauterine conditions, or unknown reasons of malformation outside of the brain. A total of 11 specimens were acquired from spontaneous abortions attributed to maternal systemic infection, pregnancy-induced hypertension syndrome, severe uterine traumas caused by accident. The specimens were first examined with ultrasound and 3.0 T MR prescans to ensure that the development status of fetal brain structures (such as the cerebrum, sulci, lateral ventricle, and corpus callosum) was anatomically normal. Maternal pregnancy records did not include documented history of fetal chromosomal abnormality, maternal genetic disease, excessive alcohol intake, smoking, and severe undernutrition, as well as eclampsia seizures. The study demographics of the specimens are listed in Table 1. The GW of the fetuses was estimated based on their crown-rump length, head circumference, foot length, and/or pregnancy records and expressed in weeks from the last menstrual period (Guihard–Costa et al. 2002). All specimens were immersed in 10% formalin for preservation without extracting the brain. The time interval between the collection of specimens and the MR scanning was within 2 months. This study was approved by the Internal Review Board of the Ethical Committee at the School of Medicine, Shandong University. Written informed consent for postmortem research was obtained from each parent.

To compare network properties of SCNs in fetal brain development with those in later neonatal development, we also included 40 healthy term-born neonates scanned at 38–42 GW, which was part of the Developing Human Connectome Project (dHCP) dataset (http://www.developingconnectome.org) (Makropoulos et al. 2018).

Table 1 Demographic information of the specimens

Gestational week	Number of subjects (total of 27)	Gender (male/female)	Termination of pregnancy
14	1	1/0	SA
16	1	1/0	SIC
17	3	2/1	SA (2), UNK
18	3	1/2	SA (2), UNK
19	4	2/2	SA (2), SIC (2)
20	5	1/4	SA (2), SIC, UNK (2)
21	6	1/5	SA (2), SIC (1), UNK (3)
22	4	1/3	SIC (2), UNK (2)

Abbreviations: SA, spontaneous abortion; SIC, stressful intrauterine conditions; UNK, unknown reasons of malformation (not brain) detected by MRI.

MRI Data Acquisition

Fetal specimens were scanned by a 7.0 T Micro-MR scanner with a maximum gradient of 360 mT (70/16 pharmaScan, Bruker Biospin GmbH, Germany) at Zhongda Hospital of Southeast University of China. A rat body coil with an inner diameter of 60 mm was selected and the axial 2D T2-weighted slice images (pixel size 0.23 mm × 0.23 mm, slice thickness: 0.5 mm with no gap) were acquired with the following parameters: TR/TE, 12 000/50 ms; field of view (FOV), 4.0 × 4.0 cm/5.0 × 5.0 cm/6.0 × 6.0 cm; matrix, 256 × 256; and NEX, 4.

Methods

Segmentation of cortical plate

The automatic segmentation of the fetal brain is challenging due to rapid morphological changes and inherently low contrast between tissues even with high-resolution images. Therefore, we manually segmented the cortical plate using Amira software based on a histology atlas of second trimester fetal brains (Bayer and Altman 2005) and previous MR studies (Kostović et al. 2002; Rados et al. 2006; Habas et al. 2010a, 2010b). The axial plane was mainly used for segmentation, with concurrent cross-check on the coronal and sagittal planes. In the high-resolution T2w MR images, the cortical plate was characterized by low intensity, while the marginal zone and subplate appeared high intensity. The inner and outer surfaces of the cortical plate were delineated using intensity differences. As shown in Figure 1, most of the primary sulci, such as the Sylvian fissure, central sulcus, and calcarine fissure, started to appear during the early second trimester.

The results of segmentation were checked and confirmed by two experienced anatomists. To check the reproducibility of our manual segmentation protocol, nine specimens were randomly chosen and resegmented by the same person at least 2 months later. The intra-class reliability was excellent with Dice's ratios of 0.9527. Illustrations of manual segmentation of several individual were shown in Figure S1.

Cortical morphological measurements: thickness, sulcation, and expansion

The segmented cortical plate surfaces were processed with CIVET MRI analysis pipeline developed at Montreal Neurological Institute (MNI). The native MR image of each subject was first corrected for nonuniformity using the N3 algorithm (Sled et al. 1998) and registered into the stereotaxic space using 9-parameter linear transformation (Collins et al. 1994). Inner and outer cortical plate surfaces were extracted from the segmented images.

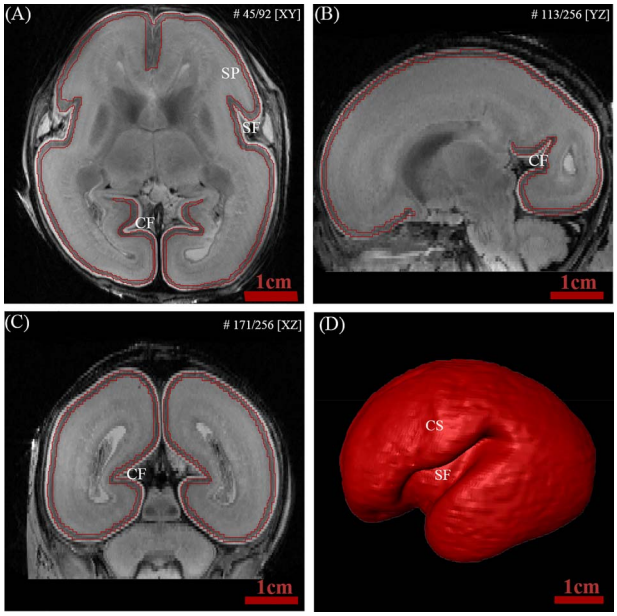

Figure 1. Example of delineation of the fetal cortical plate at 20 GW. The boundaries of the cortical plate were delineated in the axial plane (A) and confirmed in the sagittal (B) and coronal (C) planes to verify the segmentation accuracy. (D) 3D representation of reconstructed cortical plate. Abbreviations: (CF) calcarine fissure; (CS) central sulcus; (SF) Sylvian fissure; (SP) subplate.

Then, cortical plate thickness, surface area, sulcal depth, and mean curvature were extracted at 40 962 vertices per hemisphere of the brain surface. Cortical plate thickness was computed in native space using the linked distance (i.e., t-link) (Lerch and Evans 2005) between the two surfaces. The vertex-wise surface area is computed by averaging the areas of all the triangles involving the given vertex (Winkler et al. 2012). Sulcal depth was measured as a gyration/sulcation index using the NEOCIVET pipeline (Kim et al. 2016). A brain hull model was first overlaid on the cortical manifold to detect vertices on the gyral crowns (Hill et al. 2010). The crowns were initialized with a depth of zero. Sulcal depth was then calculated using the geodesic. The measures were then blurred on the surface with a 5 mm kernel due to the small brain size of fetal brain (Boucher et al. 2009; Vasung et al. 2016) to increase SNR. Smoothing was performed exclusively within the cortical area by masking non-cortical structures.

We mapped the relative cortical surface expansion on our brain template as described in Garcia et al. (2018). The map of cortical surface expansion was generated by pair-wisely dividing the mean surface area of the brains at a given age (e.g., average surface area among the fetuses in week) by the average surface area of the brains that are 1 week younger (e.g., average surface area among the fetuses in 18 week). We then computed a scalar factor as the global average cortical expansion which was computed as the mean of cortical surface expansion across vertices. Finally, the relative cortical expansion, which was measured by dividing the cortical expansion by the global average cortical expansion, was used to estimate which regions expand more than global average and which regions expand less than the global average. Garcia et al. (2018) demonstrated that brain cortical regions showing a larger relative expansion also showed more rapid folding in the third trimester. To investigate whether such a pattern is also seen in the early second trimester, we measured mean relative cortical expansions for five age groups: from 14–17 weeks to 18 weeks, from 18 weeks to 19 weeks, from 19 weeks to 20 weeks, from 20 weeks to 21 weeks, and from 21 weeks to 22 weeks, and compared them to the slope of cortical folding (mean curvature).

Template of the fetal brain

We constructed a surface template representing the age of our brain dataset using *SURFTRACC*, a surface registration algorithm included in CIVET (Robbins et al. 2004) and an unbiased template construction framework (Lyttelton et al. 2007). In brief, *SURFTRACC* first transposes individual sulcal depth maps into icosahedral spheres. It then iteratively searches for local optimal vertex correspondence between an individual and a template sphere based on a matching of a given feature (in this case, depth potential function (Boucher et al. 2009). On the cortical plate surface at the early second trimester, major sulci, such as the lateral and calcarine sulci, are only marked features that display obvious depth to constrain alignment thus likely raising concerns about alignment quality in the large intervening regions, especially since they may not expand uniformly. The deformation of the cortical areas with no marked sulcus (depth < 0.5 mm) is governed by the smoothness constraint that maintains the shape and size of triangles as regular and equal. Mapping the deformed meshes back to the original cortical surface coordinates allows a registration of the individual to the template surface. Inclusion of a regularization step further preserves local surface topology. This procedure was integrated into a hierarchical framework that allows for registration from coarse to fine scale. An initial template was created by a simple averaging of vertices among the surfaces in each age group. Thereafter, an iterative alignment proceeds from low dimensional warping of all individuals to the initial template, and toward higher dimensional warping to a new template that is constructed from the previous warping cycle as described in Lyttelton et al. (2007). Left and "flipped-right" hemispheres from all subjects were pooled to avoid subject- and hemisphere-specific bias in the evolution and averaging. For group analyses, each individual thickness map was resampled onto the template surface based on the transformation used to construct the final template.

Because little information is provided regarding the spatial distribution of sulcal depth features in fetal brains during the second trimester, it is possible that the surface registration does not work as well as it does on older brains. To validate the surface registration, cortical folding in terms of mean curvatures was also provided (Fig. 3A) for quality inspection.

Parcellation of cortical regions

The vertices on the brain surface were first grouped into 76 cortical regions based on the automated anatomical labeling (AAL). Then the seven regions of interest (ROIs) were further selected by combining the related ROIs into each of the large seven cortical regions included in the study (central, insular, frontal, parietal, occipital, temporal, and cingulate cortices). Due to the difficulty in projecting the AAL atlas from the adult brain template to fetal brains with smoother and simpler morphology, we instead used the AAL surface atlas mapped on the template representing 27–30 weeks of gestation (Kim et al. 2016). Finally, to project the atlas to current fetal brains, we registered this template to the fetal templates using SURFTRACC.

dHCP data processing

We used 40 brain MRI data of term-born neonates from dHCP dataset. These data were used as a reference in order to qualitatively and quantitatively evaluate the degree of maturation of our fetal brain data. The cortical surfaces of dHCP data were constructed using the NEOCIVET pipeline developed in our lab (Kim et al. 2016; Liu et al. 2019). The pipeline began with general data preprocessing, including denoising and intensity nonuniformity correction. Then, the brain is extracted using a patch-based brain extraction algorithm (BEaST) (Eskildsen et al. 2012) and registered to the MNI-NIH neonatal brain template (http://www.bic.mni.mcgill.ca/ServicesAtlases/NIHPD-obj2). Different types of brain tissue (GM, WM, and CSF) were thereafter segmented by an advanced label fusion based on a joint probability between selected templates (Wang et al. 2013). Next, the corpus callosum was segmented on the midline-plane and used to divide the WM into hemispheres. A marching-cube based framework was adopted to generate a triangulated mesh WM surface attached to the boundary between the GM and WM. After resampled to a fixed number of 81 920 surface meshes using the icosahedron spherical fitting, this surface was further fitted to the sharp edge of the GM-WM interface based on the image intensity gradient, which preserves the spherical topology of the cortical mantle. A CSF skeleton was then generated from the union of WM and CSFs. The pial surface was constructed by expanding the WM surface toward the skeleton as an intermediate pial surface. The intermediate pial surface further underwent a fine deformation to identify actual edges of sulcal CSF volumes using an intensity gradient feature model. Finally, cortical thickness was estimated based on the Euclidean distance between the white matter and pial surface.

SCN construction

We used cortical plate thickness values to construct SCNs for two groups of subjects corresponding to fetuses during the early second trimester and term neonates. A general linear model (GLM) was performed to calculate the statistical similarity in cortical plate thickness between two vertices across subjects while accounting for gestational age. A correlation matrix computed across all 81 924 vertices is extremely computationally expensive. On top of that, there is no digital fetal brain atlas which can be referred to when parcellating the early fetal brain. Thus, the study implemented a template-free approach, which was validated in previous studies that evenly parcellated the cortex into regions of similar size (Tymofiyeva et al. 2012; Meng et al.

2015), avoiding any imposing anatomical bias. Thus, we uniformly sampled 1284 vertices for the two hemispheres, which represented network nodes (Kim et al. 2020). An illustration of node distribution was shown in Figure S2.

Network Analysis

For graph-theoretical analysis, correlation matrices were first binarized based on sparsity thresholding. Sparsity was defined as the total number of edges in a graph divided by the maximum possible number of edges. A fixed sparsity-specific threshold (for instance, χ threshold implied χ of the topmost connections preserved) assured the same number of edges for graphs of different groups (Achard and Bullmore 2007). The 9% threshold was chosen to ensure that all nodes connected to at least one other node. To characterize the development of the topological organization and SCNs from the early second trimester to birth, the following characteristic graph theory metrics were calculated:

Nodal properties

We first used the nodal degree centrality to explore age-related changes in nodal properties between fetal and neonatal groups. For a given node, its degree centrality indicated the number of edges connecting it with all other nodes. Nodes with high degrees ($>$mean $+ 2$ SD) were defined as hubs, which exhibited high connectivity to proximal nodes (likely in the same local community) and remote nodes (in different communities) of the brain (Cao et al. 2017). We compared the degree distributions of nodes, the regional pattern of nodal degree, and the number of hubs between fetal and neonatal groups.

Global network organization

To compare the global topological properties of the two groups, we computed the clustering coefficient C_p, the shortest path length L_p, and their normalized metrics (γ and λ, respectively) after comparison with a set of randomized networks. Module detection was performed to identify parcellations of the brain network into different modules (Newman 2006), which indicated subsets of nodes that were more highly interconnected but less connected to nodes in different modules. The modularity was defined as the largest value of modularity measures associated with all possible configurations of modules, which could be found by optimization algorithms (Newman and Girvan 2004). The most representative and stable network partition was determined by consensus clustering in the networks (Lancichinetti and Fortunato 2012; Bienkowski et al. 2018). We examined the change of modularity across the two groups. We measured the Euclidean distance between each pair of connected nodes. The distance of each group was defined as the average distance of all edges and normalized to remove the effect of different brain size.

Statistical Analysis

All statistical analyses were performed using SurfStat (http://www.math.mcgill.ca/keith/surfstat/) for the analysis of cortical plate thickness and Brain Connectivity Toolbox (https://sites.google.com/site/bctnet/) for the analysis of covariance network. Linear regression analysis was performed to measure the correlation between the average thickness of the whole brain and increasing gestational age. The vertex-based regression analysis was also performed. A t-test was used to examine the thickness differences between the left and right hemispheres.

To determine the statistical comparison in network properties between two groups, we used a nonparametric permutation test procedure (He et al. 2008; Khundrakpam et al. 2017). In order to test the null hypothesis that any observed group differences could occur by chance, each subject's set of cortical plate thickness values were randomly reallocated into two groups. The number of subjects within each group was the same as two groups in real conditions. Then, the correlation matrix was constructed and binarized using the same sparsity threshold as in the construction of real brain networks. Network properties were then computed for each randomized group. The randomization procedure was repeated 1000 times and the 95 percentile points for each distribution were used as the critical values for a one-tailed test of the null hypothesis with a probability of type I error of 0.05. In this study, the above procedure was used to compare group differences in topological properties (normalized cluster coefficient, normalized shortest path, modularity, and mean European distance). The false discovery rate (FDR) procedure was performed to correct the multiple comparisons at a q value of 0.05.

Data Availability

All cortical surface features and the surface template utilized in the current study can be found in https://github.com/bigting84/fetus-surface. Our native MRI images will be made available on request from any qualified investigator who provides a practicable proposal, or for the purpose of replicating procedures and results presented in the current study.

Results

Thickness of Cortical Plate

The thickness of the cortical plate increased significantly throughout the whole brain during 14 to 22 GW ($P < 0.001$; Fig. 2B). There was no significant difference in thickness between left and right hemispheres ($P > 0.1$).

In addition, we provided the maps of mean cortical thickness for each age group in Figure 2A. The thickness of the cortical plate underwent uneven increases across different cortical regions. It is clear that the cortical thickness trajectory is consistent with what was found in the literature: cortical growth starts from the central cortex and expands to both frontal and parietal/temporal regions (Garcia et al. 2018). A standard deviation (STD) map and STD-mean thickness ratio map for each age group are also shown in Figure S3. The STD and STD-mean ratio maps demonstrated that the regional variability among the analyzed individual data was much smaller than the mean value of cortical thickness for all the age groups. This suggests that the cortical thickness feature we extracted from the high-resolution ex vivo MRI was reliable and reflected reasonable cortical growth after applying a proper smooth kernel size. An illustration of cortical thickness for individual brains from 14–22 GW is shown in Figure S4.

Sulcal Depth and Mean Cortical Curvature

Compared to cortical thickness, mean curvature and sulcal depth did not show significant increases or decreases throughout the period between 14 and 22 GW ($P > 0.05$), indicating that a lack of consistent folding occurs in the early second trimester. According to spatiotemporal maps of mean curvature and sulcal depth shown in Figure 3A and B, it was clear that most

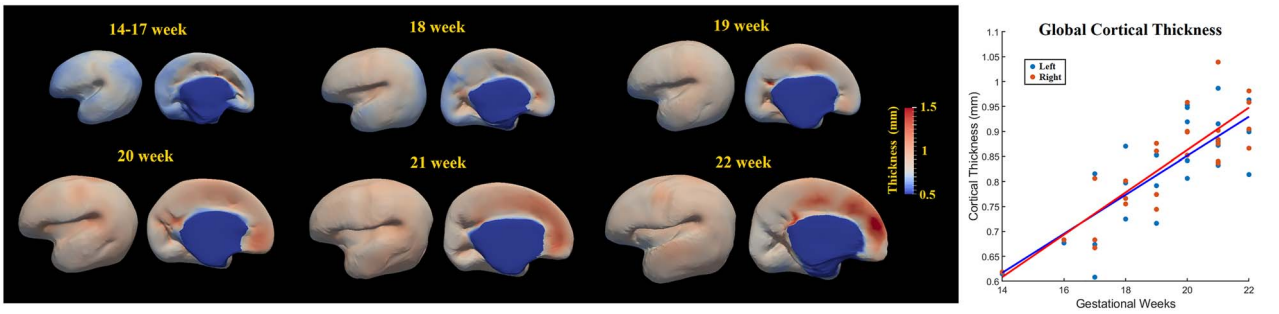

Figure 2. Developmental pattern of the thickness of cortical plate during the early second trimester. Spatiotemporal maps of cortical plate thickness at 14–17, 18, 19, 20, 21, and 22 weeks displayed on the corresponding age-specific templates (left panel). The mean cortical plate thickness of left hemisphere (blue) and right hemisphere (red) increased linearly with gestational weeks (right panel).

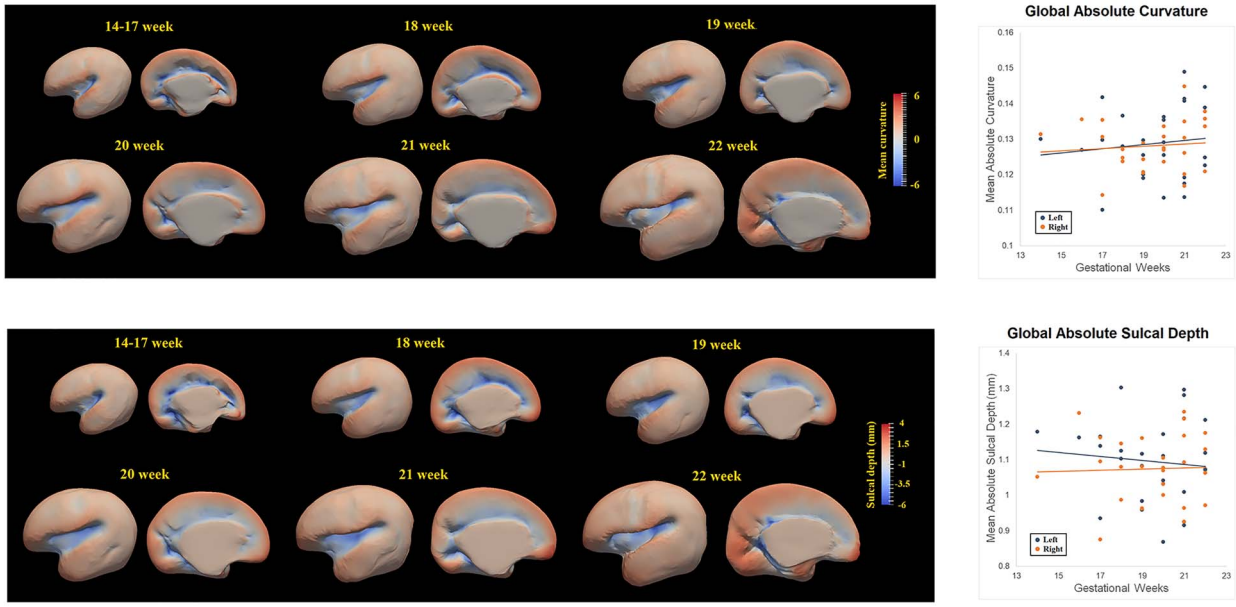

Figure 3. Developmental pattern of mean curvature and sulcal depth of cortical plate during the early second trimester. Spatiotemporal maps of mean curvature and sulcal depth of cortical plate at 14–17, 18, 19, 20, 21, and 22 weeks displayed on the template (left panel). Scatter plots showing the correlations between mean curvature and sulcal depth of two hemispheres and gestational age in weeks (right panel).

cortical regions did not show a significant folding trajectory, other than folding occurring in major sulci, such as Sylvian fissure, cingulate sulcus, and calcarine sulcus. Furthermore, significantly decreased folding was found in the cingulate cortex area. There was no significant difference in mean curvature and sulcal depth between left and right hemispheres ($P > 0.05$). An illustration of mean curvature for individual brains from 14–22 GW was shown in Figure S5.

Cortical Growth Rate

We further analyzed growth rates in terms of cortical thickness, surface area, and mean curvature. Developmental trajectories and spatiotemporal maps of cortical thickness, surface area, and mean curvature are displayed in Figure 4. To quantify changes over time, local growth rates (n = 27 subjects) were plotted over different gestational weeks in seven typical cortical regions by averaging each of the cortical features for all the vertices within each ROI per hemisphere (left: blue, right: red, Fig. 4A). The seven ROIs selected were central, insular, frontal, parietal, occipital, temporal, and cingulate cortices (Fig. 4 top row). We further showed an illustration of seven ROIs for individual brains from 14–22 GW in Figure S6. We observed that for cortical thickness and surface area, all cortical regions displayed significant trends in growth rate (corrected $P < 0.05$). For mean curvature, however, only the central cortex and occipital cortex showed significantly increased folding over time. In addition, the cingulate cortex also exhibited a significantly decreased folding trajectory. Linear regression analysis indicated that for cortical thickness, the growth rates in the frontal cortex (average $\beta = 0.061$ mm/week) and cingulate cortex (average $\beta = 0.049$ mm/week) were slightly faster than those of other cortical regions (mean $\beta = 0.040$ mm/week) due to the faster growth of cortical regions near the medial superior frontal cortex. For surface area, the insula (average $\beta = 0.015$ mm^2/week) and cingulate cortex (average $\beta = 0.015$ mm^2/week) expanded faster than other

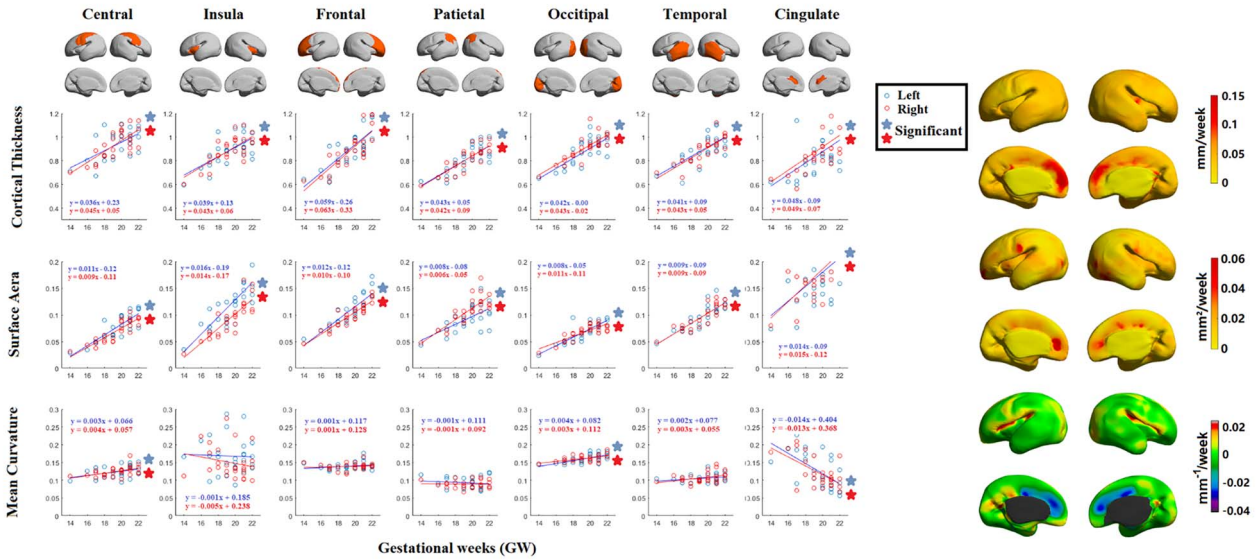

Figure 4. The developmental trajectory of mean cortical thickness, surface area, and mean curvature of left hemisphere (blue) and right hemisphere (red) in central cortex, insula, frontal cortex, parietal cortex, occipital cortex, temporal cortex, and cingulate cortex (left panel). The growth rate of cortical thickness, surface area, and mean curvature of cortical plate from 14 to 22 GW was, respectively, mapped on the template (right panel).

areas (mean β = 0.009 mm^2/week). For mean curvature, all areas generally fold slowly in this period of development. However, the central cortex (average β = 0.004 mm^{-1}/week) and occipital cortex (average β = 0.004 mm^{-1}/week) exhibited relatively faster folding, which were significant (mean β = 0.001 per week on other ROIs), representing the emergence of sulci in the motor and primary visual cortices during the second trimester. In addition, the cingulate cortex (average β = −0.015 mm^{-1}/week) exhibited significantly decrease of folding, representing the de-sulcation process in the cingulate cortices during the second trimester.

Cortical Expansion

We found that the regions showing a relatively large expansion overlapped or were proximal to regions showing a fast-folding trajectory (Fig. 5). These regions include main sulci, such as the Sylvian fissure, and central, parietooccipital, and calcarine sulci, which are prominent folding features in this developmental period.

Structural Covariance Network

Nodal degree distribution

Due to the effects of the differences in the MRI field strength (7 T vs 3 T) and scanner, as well as the difference in tissue segmentation approaches (manual segmentation vs. automated segmentation), it is noteworthy that there may be inaccurate results when conducting a direct statistical comparison between fetal brain data and neonatal data. Hence, we only provide a qualitative description of the results here but document the statistical comparisons separately in the Supplementary section (Fig. S7) for readers' information and interest.

The exploration of the nodal degree centrality demonstrated that the nodal degree in fetal group exhibited an uneven distribution with one short tail fading to the right side (Fig. 6A). The distribution curve also showed that almost equal number of nodes in the early second trimester exhibited a nodal degree between 3% and 15%, which suggested the brain development in early second trimester does not generate a topologically well-organized network as found in adult brains; the term-born neonatal group displayed a skewed and heavy-tailed node degree distribution, which tended to follow an exponentially truncated power law. Compared to fetal brain, the distribution curve in term neonates exhibited a larger number of hubs (very high nodal degree) and a larger number of leaves (very low nodal degree; Fig. 6A), which is more like the network in adult brain. This reflected in term-born neonates, the node roles in brain network start to differentiate in comparison to fetal brain, i.e., some nodes became increasingly influential as hubs, whereas other nodes became increasingly insignificant throughout brain development.

It is shown that the numbers of low-degree nodes (connected to <3% nodes of the network) and high-degree nodes (connected to >20% nodes of the network) were greater in the term group compared to the fetal group, while the number of moderate-degree nodes (connected to 5%–15% nodes of the network) was greater in the fetal group (Fig. 6A). The number of hubs in the fetal group (N = 76) was observed to be fewer than that in the term group (*vs.* N = 112, Fig. 6B). We further mapped hub regions for both the second trimester and term group (Fig. 6C) for qualitative evaluation. We found that in the early second trimester, hubs were found mainly in frontal, parietal, and temporal lobes; the SCN hubs for term-born neonates were found primarily distributed in insular and inferior frontal regions.

Global network properties

Global network properties of our fetal brain data as well as neonatal data are shown in Table 2 as reference. Again, we provide the results of statistical comparisons in these properties separately in Supplementary data (Fig. S7) for readers' information. Qualitatively, the fetal brain data analyzed in the current study generally displayed a less integrated (longer global

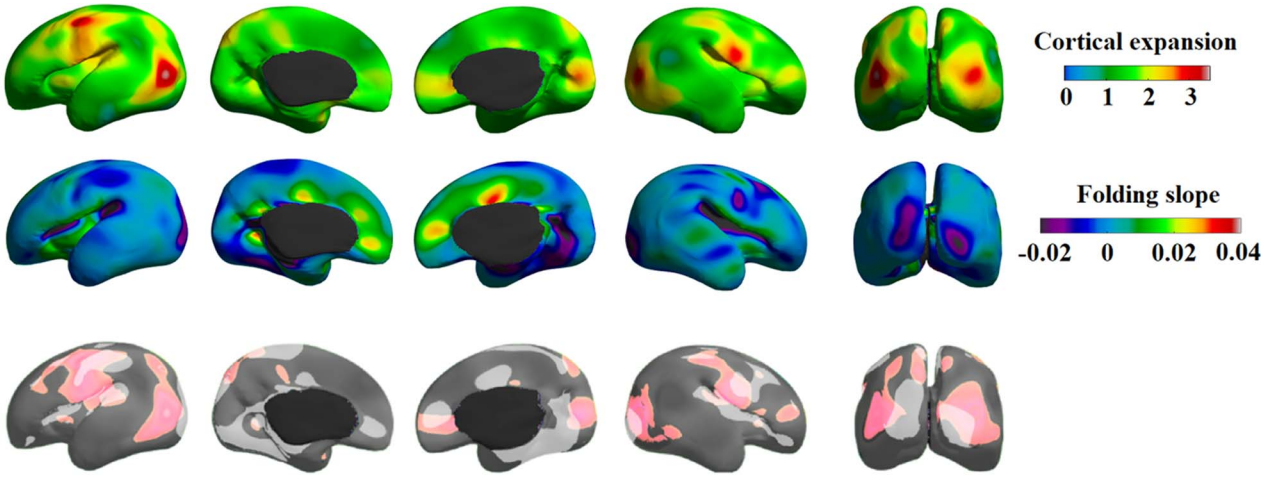

Figure 5. Gradients of cortical expansion (top) and folding slope (bottom). The upper panel shows the average of all five cortical expansions representing the expansion pattern over the entire age range. Areas with a negative folding slope present sulcation, whereas those with a positive slope present gyration (or sulcal flattening found in the cingulate cortex). Cortical expansion partially overlapped with the regions that have apparent folding features in this developmental period (lower panel).

path length) and more segregated (higher normalized clustering coefficient, larger modularity) network compared to dHCP term neonates.

Moreover, we calculated the mean Euclidean distance (normalized to same brain template) between pairs of connected nodes for the two groups. The mean distance of the neonatal group was higher than that of the fetal group (D_{term}= 34.12 mm, D_{2nd}= 27.13 mm). Results suggested that the strongest connections in the fetal brain were predominantly characterized by short-range connections, signifying anatomical proximity. A greater proportion of strongest connections were established between long-distance brain regions in newborn babies.

We further compared the distribution of nodal mean shortest path length by averaging the shortest path length from each node in network to all the others. The changing patterns of nodal path length were similar to those of the nodal degree (Fig. 6*A* and *D*). That is, the numbers of nodes with shorter mean path lengths ($1.5 \leq L \leq 1.7$) and longer mean path lengths ($L > 2.8$) were found to be increased in the term group, while the number of nodes with moderate mean path lengths ($1.8 < L \leq 2$) was increased in the fetal group (Fig. 6*D*).

Younger (<20 weeks) vs. older group (≥20 weeks)

To assess possible temporal changes of SCNs in the early second trimester, we further divided the fetal subjects into two groups: younger group (< 20 GW) and older group (≥ 20GW), and constructed SCNs for the two groups. Network properties between the two groups had no significant differences with detailed results provided in the Supplemental Table S1.

Discussion

In the present study, we reported the morphological development of the cortical plate during the early second trimester and explored the SCN from the early second trimester to birth. The cortical plate displayed significant increases in thickness and expansions in area throughout all regions from 14 to 22 GW. The analysis of mean curvature and sulcal depth showed that other than folding occurring in major sulci, such as the Sylvian fissure, cingulate sulcus, and calcarine sulcus, most cortical regions did not present significant folding trajectory throughout the period. Moreover, when comparing network properties of the fetal group with the neonatal group, we showed that the topological architecture of the SCN changed as the brain developed. In the fetal group, the network was characterized by a similar node-degree, similar average shortest path length, physically short connections between nodes, and higher modularity. By contrast, the neonatal group exhibited a right-tailed degree distribution, the emergence of shorter and longer average shortest path lengths, and increasing Euclidean distances between pairs of connected nodes. Such findings may suggest that the brain network was still in its primitive state during the early second trimester. The covariance of cortical thickness in the early second trimester may not be differentiated sufficiently to a biologically meaningful biomarker that fully represents brain network organizations. On the contrary, structural covariance at term newborns may represent biologically meaningful communications between pairs of brain regions, which indicates a more sophisticated, integrated, and efficient network system.

Cortical Plate Thickness

During the early fetal period, neurons are generated in the ventricular and subventricular zones and migrate toward the cortical plate along the radial glial fibers. Once neurons reach their destination in the cortical plate, they begin to extend their axonal, dendritic, and synaptic projections (Rakic 1972, 2003; Kwan et al. 2012). The majority of neurons finish their migratory activity by the end of gestational age 20–21 weeks (Bystron et al. 2008). A previous study showed that the cortical plate thickness increased from 0.86 to 2.6 mm during the late second trimester of gestation (20–26 GW) (Corbett-Detig et al. 2011). Using ex vivo high-field 7 T MRI, the current study had an ability to demonstrate that the average thickness of the cortical plate linearly increased approximately from 0.6 to 1.1 mm during the early second trimester (14–22 GW), providing evidence that the early fetal cortical growth originated from an earlier period of neurodevelopment than previous studies observed.

Based on our findings on surface area and thickness (Fig. 4), the insula, the primary visual cortex, orbitofrontal cortex, and

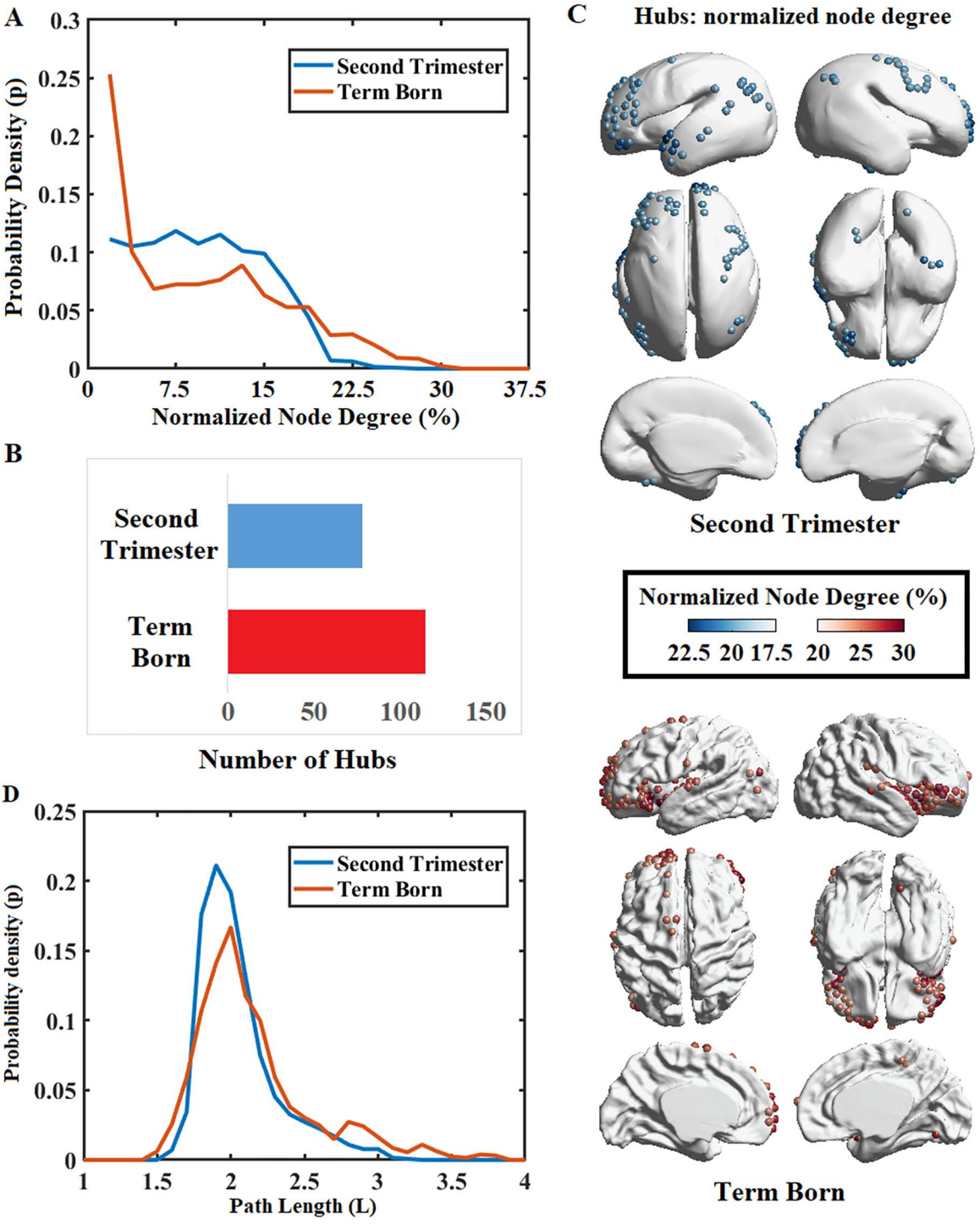

Figure 6. Distributions of nodal degree and nodal mean shortest path length of SCNs for brains scanned at early second trimester and at term. (A) Normalized distribution curve of node degree for the two groups, normalized by number of nodes in networks. (B) Number of hubs significantly increased in the term-born group. (C) Regional distribution of hubs for the two groups. (D) The distribution curve of nodal mean shortest path length for the two groups.

cingulate showed relatively high growth rate. Previous studies reported that neurogenesis and cortical plate maturation occurred earliest in areas close to the insula (Sidman and Rakic 1982; Smart et al. 2002; Afif et al. 2007). In addition, we found faster development in the cingulate cortex, which belongs to the limbic system (the "visceral brain"). In our previous study, the fetal hippocampus, as a main part of the limbic system, developed earlier than other brain regions during the same stages investigated (Ge et al. 2015). Our results were also consistent with those of morphological development after 20 GW. Rajagopalan et al. (2011) found that regions near the insula, cingulate, and orbital sulcus were characterized with above-

Table 2 Global network properties of structural covariance networks for fetal and neonatal groups

	Clustering coefficient C_p	Normalized C_p	Path length L_p	Normalized path length L_p	Modularity	Normalized distance
Second trimester	0.543	3.735	2.106	1.416	0.301	27.13 mm
Term born	0.577	1.511	2.001	1.376	0.172	34.12 mm

average growth rate of volume between 20–24 and 24–28 GW. Xia calculated brain surface area of normal fetuses at 26–29 GW and found that orbitofrontal and anterior cingulate regions of the two hemispheres presented relatively low growth rate of surface area (Xia et al. 2019). Garcia et al.'s (2018) cortical expansion study of preterm infants (28–38 postmenstrual weeks) found lower relative expansion at the medial frontal and insular regions.

A prior work by Vasung et al. (2016) also investigated cortical plate and subplate thicknesses and volumes from postmortem brain specimens and analyzed structural correlations between regions. Their work based on ex vivo 3 T MRI with a large age range of 13–40 weeks of gestation, a high image resolution, surface-based morphometric analysis using cortical thickness and area, and cortico-cortical correlation of these measurements has a common with the current study. Yet, there are numerous differences between two studies, making both works unique to enlarge our knowledge of fetal neurodevelopment. Our study was based on 7 T MRI with a higher image resolution (0.5 mm isotropic for 15 GW or older vs. $0.23 \times 0.23 \times 0.5$ mm). We also analyzed the covariance of cortical thickness using graph theory approaches. On the other hand, Vasung and colleagues' work included histology data for the analysis of different cytoarchitectures. It is also noteworthy that while Vasung and colleague's work focused on the difference in maturation between thee cortical plate and subplate, we focused on the various aspects of maturation in cortical plate by analyzing various morphological measurements and SCN.

Cortical Folding

For cortical folding, or more specifically mean curvature, the central and occipital cortex exhibited faster cortical curving or increasing cortical folding, representing the emergence of sulcus in the motor and primary visual cortex during the early second trimester. Particularly, the Sylvian fissure, central sulcus, calcarine fissure, and the parieto-occipital sulcus emerge. In our analysis, we also found cortical folding in the central and occipital cortex, which is in accordance with previous studies (Huang et al. 2009), although some prior studies also reported that the main sulcus appears starting from around 20 gestation weeks (Chi et al. 1977). Due to the small sample size, the difference might be caused by individual differences due to genetic or epigenetic factors i.e., environmental effects, disease pathology, or hereditary effects, etc. (Zhang et al. 2013).

It is also worth noting that in the cingulate cortex, a positive developmental trend of curvature was observed, indicating that cortical folding is decreasing during this period. This peculiar morphological change of the cingulate gyrus has already been documented in histological sections (Bayer and Altman 2005) (Fig. S8) and is visually well recognized in our MRI data (Fig. S9). The cingulate gyrus is one of the main parts of the limbic system, which regulates visceral activities and belongs to the archicortex and paleocortex in evolution criteria. Phylogenetically older cortical areas, such as the cingulate cortex, mature earlier than newer cortical regions. It is possible that the rapid development of cingulate cortex and decreases in volume of the lateral ventricle cause the decrease in the depth of the cingulate gyrus during the early second trimester. The real sulcation process of cingulate cortex starts after 22 GW from the late second trimester, forming the adult-like cingulate sulcus (Bayer and Altman 2003).

Cortical Expansion

Garcia et al. (2018) demonstrated that the highest cortical expansion occurs in areas that undergo the most dramatic folding in the third trimester. We found that regions showing a larger relative expansion overlapped or were proximal to the regions showing faster folding trajectory. These regions include main sulci, lateral and calcarine sulci, which are prominent folding features in this developmental period. These consistent findings on the relationship between cortical expansion and cortical folding suggest that the physical expansion of the cortex leads to mechanical instability and folding in different areas at different times (Garcia et al. 2018). In addition, we found that many areas are not fully accordant (Fig. 5 lower panel), suggesting that the expansion of cortical area does not result solely from gyration/sulcation but also from other factors such as regional growth volume.

Structural Covariance Network

We observed that the degree distribution of the network nodes changed from an uneven distribution with one short tail at the early fetal period to a right-tail shape at birth (Fig. 6*A*). In previous studies, the exponentially truncated power-law distribution of node degrees was found at preterm around 30 GW and at term (Ball et al. 2014; van den Heuvel et al. 2015). The changing pattern of nodal mean path length was similar to that of degree distribution (Fig. 6*D*). In the fetal group, most nodes exhibited similar mean shortest path lengths, while in the neonatal group, nodes exhibited both shorter and longer path lengths. Nodes with a shorter path length may indicate the presence of more hubs. Some nodes had increased path lengths, which were representative of leaf nodes in the network, or even the leaf of leaf nodes in the network. At the early state of covariance network formation, most nodes were characterized by similar degrees and shortest path length. As the fetal brain structural covariance connectivity underwent reorganization throughout development, the broad-scale distributions of node degrees and shortest path lengths emerged in the neonatal network. The connectome was characterized by sparsely connected nodes with longer mean path lengths and densely connected nodes with shorter path lengths. Additionally, the number of hubs increased throughout brain network development from the early second trimester to birth (Fig. 6*B*). Because hubs indicate high functional connectedness

to other regions of the brain, the increasing presence of hubs by term age suggests that the early developing brain grows as a system with increasing integration and efficiency, forming the foundation for various aspects of complex cognitive function. Given that the nature of fetal brain hubs rapidly reshapes in terms of their location, role, and number, the fetal brain may be highly vulnerable to insults and abnormal connectivity (Crossley et al. 2014; Aerts et al. 2016), thereby urging important clinical attention on the spatiotemporal pattern of network properties throughout brain development. In the term-born neonates group, node with high degree was found mostly distributed in insula and inferior frontal cortex (Fig. 6C). Ball et al. (2014) also found that the hub regions mainly expand into those two regions from 30 to 40 GW. The reorganization of topological distribution suggested the differentiation of node roles in the network. Some nodes became increasingly influential as hubs, whereas other nodes became increasingly insignificant throughout brain development. With the increasing formation of distinct hub architecture, the fetal brain network may be preparing for higher order cognitive functioning that manifests in later adolescence.

We observed that the modularity became lower from the early second trimester to birth. From Thomason et al.'s (2014) study, the modularity of functional brain network existed as early as approximately 20 GW and decreased with increasing gestational age. Therefore, structural and functional systems may be rather independent of each other in the early period of fetal development, which is characterized by highly modular and local networks. Such local community networks evolve rapidly with a significant decrease in modularity during prenatal and postnatal development (Tymofiyeva et al. 2013; Huang et al. 2015). In particular, the strengthening of inter-modular connections combined with the weakening of intra-modular connections results in the decrease of modularity, representing the growth of network integration capacity.

We found that the mean Euclidean distance between pairs of connected nodes was significantly higher in the term neonatal group. In previous studies, long-range association pathways were also observed to increase with fetal age using DTI tractography method (Kostovic and Jovanov-Milosevic 2006; Takahashi et al. 2014) and functional connectome (Thomason et al. 2015). The increasing proportion of long-distance thickness covariance connections, combined with the change of module distribution, indicates the evolution of a local-to-distributed brain network architecture during early fetal and neonatal development. Such trends are also supported in other modal connectivity studies, as functional and structural brain networks develop from a local to more distributed organization (Fair et al. 2009; Yap et al. 2011).

As largely discussed in literature (Alexander-Bloch et al. 2013a; Evans 2013), it has been widely accepted that the SCNs in developing brains is related to the functional organization of the brain rather than the structural connectivity. Accordingly, the regional variability of cortical morphology largely implicates functional organization and segregation in pediatric and adult brains (Fischl et al. 2008; Glasser and Van Essen 2011). However, the biological meaning of the SCNs at the second trimester of gestation remains unclear. Given that neurons actively proliferate, then migrate from the periventricular germinal matrix to the cortex along the radial pathway throughout the second trimester and beyond, the correlation of cortical thickness between two cortical regions revealed in our data might account for the reciprocal relationship among actively forming cortical plates, which is governed by the rate of neural proliferation and migration (Gressens 2000; Hirota and Nakajima 2017). In other words, the two regions displaying a high correlation in thickness likely explain their synchronous cortical structural maturation led by the aforementioned neural development process. However, it is noteworthy that this reasoning is inconclusive and limited by our data's relatively macroscopic resolution (sub-millimetric) and the morphological metric that is not specific to the dynamic changes reflecting either the neural migration or proliferation.

Limitations and Future Directions

There are several limitations to our study. First, our sample size is relatively small with few subjects representing each gestational week, especially for the younger weeks of the second trimester. This is a common problem in fetal specimens imaging, given that fetal specimens are extremely difficult to obtain (Huang et al. 2009; Vasung et al. 2016). Second, there could be minor tissue degradation caused by formalin fixation, which is also a common problem in postmortem studies (Stan et al. 2006) and may slightly affect thickness measurements. In order to mitigate such problems, this study acquired MR images of the brain inside the skull, and the time interval between the collection of specimens and MRI scanning was less than 2 months. Third, unlike networks derived from white matter pathways or functional correlation, SCN is a statistical construct that only indirectly represents theoretic pathways of maturational information transfer. Despite its limitations, however, anatomical covariance likely reflects synchronized development of brain structure and function, while providing complementary characteristics of brain connectivity (Evans 2013). Moreover, covariance network analyses were scientifically favored and widely used to characterize trophic pathways of the developing brain where morphological growth was vigorous (Fan et al. 2011; Alexander-Bloch et al. 2013b; Nie et al. 2014; Geng et al. 2017). Previous studies of SCNs mostly focused on neurodevelopmental patterns of postnatal children and adults, in which cortical thickness maps were used to show robust regional variability relating to functional organization (Geng et al. 2017; Scheinost et al. 2017). To what extent that structural covariance represents functional connectivity, or even anatomical connectivity, in the early second trimester, needs to be further investigated. Reinterpretation of the current study's findings may be needed if functional relationships were found. To our knowledge, our study represents the first attempt to construct SCNs for fetuses at extremely early development stages, which may lay the foundation for future works that combine cellular-level immunohistochemistry with in vivo neuroimaging to evaluate the reproducibility or interpretations/hypotheses proposed by our work. Lastly, due to the absence of fetal data during the late second and third trimesters, a longitudinal study continuing throughout those periods are not able to be executed. In the future, more fetal data should be collected to better characterize early development of the brain and covariance networks of the prenatal period.

Conclusion

With 7.0 T high-resolution MR images of fetal brains from 14 to 22 GW, we quantified the morphological development patterns of cortical plate and constructed SCNs. The cortical plate displayed significant increases in thickness and expansions in area throughout all regions but changes of curvature in only certain major sulci. Though the fetal brain structural network exhibited

modularity property during the early second trimester, this network was still considered to be in a primitive form compared to a more efficient and well-integrated neonatal network. Ultimately, the brain connectome experienced rapid development and reorganization throughout the prenatal period toward the healthy newborn brain. As many neurological disorders manifesting later in life may originate in the prenatal neurodevelopmental period, our findings are thereby importantly pertinent to the urgent clinical and scientific demand in characterizing fetal brain development.

Supplementary Material

Supplementary material can be found at *Cerebral Cortex* online.

Funding

This work was supported by the National Natural Science Foundation of China (grant numbers 31771328, 31571237, 31872802, 81801776) and Major Scientific and Technological Innovation Projects of Shandong Province (grant number 2017CXGC1501), in part by Natural Science Foundation of Jiangsu Province (grant number BK20170256), and the National Institutes of Health grants (grant numbers P41EB015922, U54EB020406).

Notes

We would like to thank Zhongda Hospital of Southeast University for MRI scans of fetal specimen. We are also thankful to the Developing Human Connectome Project. *Conflict of Interest*: The authors have no conflicts of interest to declare.

References

Achard S, Bullmore E. 2007. Efficiency and cost of economical brain functional networks. *PLoS Comput Biol*. 3:e17.

Aerts H, Fias W, Caeyenberghs K, Marinazzo D. 2016. Brain networks under attack: robustness properties and the impact of lesions. *Brain*. 139:3063–3083.

Afif A, Bouvier R, Buenerd A, Trouillas J, Mertens P. 2007. Development of the human fetal insular cortex: study of the gyration from 13 to 28 gestational weeks. *Brain Struct Funct*. 212:335–346.

Alexander-Bloch A, Giedd JN, Bullmore E. 2013a. Imaging structural co-variance between human brain regions. *Nat Rev Neurosci*. 14:322–336.

Alexander-Bloch A, Raznahan A, Bullmore E, Giedd J. 2013b. The convergence of maturational change and structural covariance in human cortical networks. *J Neurosci*. 33:2889–2899.

Ball G, Aljabar P, Zebari S, Tusor N, Arichi T, Merchant N, Robinson EC, Ogundipe E, Rueckert D, Edwards AD et al. 2014. Rich-club organization of the newborn human brain. *Proc Natl Acad Sci U S A*. 111:7456–7461.

Batalle D, Hughes EJ, Zhang H, Tournier JD, Tusor N, Aljabar P, Wali L, Alexander DC, Hajnal JV, Nosarti C et al. 2017. Early development of structural networks and the impact of prematurity on brain connectivity. *Neuroimage*. 149:379–392.

Bayer SA, Altman J. 2003. *The Human Brain During the Third Trimester*. Indianapolis: CRC Press.

Bayer SA, Altman J. 2005. *The human brain during the second trimester (Atlas of the human central nervous system development)*. Indianapolis: CRC Press.

Bendersky M, Tamer I, Van Der Velde J, Dunaievsky A, Schuster G, Rugilo C, Sica RE. 2008. Prenatal cerebral magnetic resonance imaging. *J Neurol Sci*. 275:37–41.

Bienkowski MS, Bowman I, Song MY, Gou L, Ard T, Cotter K, Zhu M, Benavidez NL, Yamashita S, Abu-Jaber J et al. 2018. Integration of gene expression and brain-wide connectivity reveals the multiscale organization of mouse hippocampal networks. *Nat Neurosci*. 21:1628–1643.

Boucher M, Whitesides S, Evans A. 2009. Depth potential function for folding pattern representation, registration and analysis. *Med Image Anal*. 13:203–214.

Brown CJ, Miller SP, Booth BG, Andrews S, Chau V, Poskitt KJ, Hamarneh G. 2014. Structural network analysis of brain development in young preterm neonates. *Neuroimage*. 101:667–680.

Bystron I, Blakemore C, Rakic P. 2008. Development of the human cerebral cortex: boulder committee revisited. *Nat Rev Neurosci*. 9:110–122.

Cao M, He Y, Dai Z, Liao X, Jeon T, Ouyang M, Chalak L, Bi Y, Rollins N, Dong Q et al. 2017. Early Development of functional network segregation revealed by Connectomic analysis of the preterm human Brain. *Cereb Cortex*. 27:1949–1963.

Chi JG, Dooling EC, Gilles FH. 1977. Gyral development of the human brain. *Ann Neurol*. 1:86–93.

Collins DL, Neelin P, Peters TM, Evans AC. 1994. Automatic 3D intersubject registration of MR volumetric data in standardized Talairach space. *J Comput Assist Tomogr*. 18:192–205.

Corbett-Detig J, Habas PA, Scott JA, Kim K, Rajagopalan V, McQuillen PS, Barkovich AJ, Glenn OA, Studholme C. 2011. 3D global and regional patterns of human fetal subplate growth determined in utero. *Brain Struct Funct*. 215:255–263.

Crossley NA, Mechelli A, Scott J, Carletti F, Fox PT, McGuire P, Bullmore ET. 2014. The hubs of the human connectome are generally implicated in the anatomy of brain disorders. *Brain*. 137:2382–2395.

Doria V, Beckmann CF, Arichi T, Merchant N, Groppo M, Turkheimer FE, Counsell SJ, Murgasova M, Aljabar P, Nunes RG et al. 2010. Emergence of resting state networks in the preterm human brain. *Proc Natl Acad Sci U S A*. 107:20015–20020.

Dubois J, Benders M, Cachia A, Lazeyras F, Ha-Vinh Leuchter R, Sizonenko SV, Borradori-Tolsa C, Mangin JF, Huppi PS. 2008. Mapping the early cortical folding process in the preterm newborn brain. *Cereb Cortex*. 18:1444–1454.

Eskildsen SF, Coupe P, Fonov V, Manjon JV, Leung KK, Guizard N, Wassef SN, Ostergaard LR, Collins DL, Neuroimaging ASD. 2012. BEaST: Brain extraction based on nonlocal segmentation technique. *Neuroimage*. 59:2362–2373.

Evans AC. 2013. Networks of anatomical covariance. *Neuroimage*. 80:489–504.

Fair DA, Cohen AL, Power JD, Dosenbach NU, Church JA, Miezin FM, Schlaggar BL, Petersen SE. 2009. Functional brain networks develop from a "local to distributed" organization. *PLoS Comput Biol*. 5:e1000381.

Fan Y, Shi F, Smith JK, Lin W, Gilmore JH, Shen D. 2011. Brain anatomical networks in early human brain development. *Neuroimage*. 54:1862–1871.

Fischl B, Rajendran N, Busa E, Augustinack J, Hinds O, Yeo BT, Mohlberg H, Amunts K, Zilles K. 2008. Cortical folding patterns and predicting cytoarchitecture. *Cereb Cortex*. 18:1973–1980.

Garcia KE, Robinson EC, Alexopoulos D, Dierker DL, Glasser MF, Coalson TS, Ortinau CM, Rueckert D, Taber LA, Van Essen DC

et al. 2018. Dynamic patterns of cortical expansion during folding of the preterm human brain. *Proc Natl Acad Sci U S A*. 115:3156–3161.

Ge X, Shi Y, Li J, Zhang Z, Lin X, Zhan J, Ge H, Xu J, Yu Q, Leng Y et al. 2015. Development of the human fetal hippocampal formation during early second trimester. *Neuroimage*. 119:33–43.

Geng X, Li G, Lu Z, Gao W, Wang L, Shen D, Zhu H, Gilmore JH. 2017. Structural and maturational covariance in early childhood Brain Development. *Cereb Cortex*. 27:1795–1807.

Glasser MF, Van Essen DC. 2011. Mapping human cortical areas in vivo based on myelin content as revealed by T1- and T2-weighted MRI. *J Neurosci*. 31:11597–11616.

Gressens P. 2000. Mechanisms and disturbances of neuronal migration. *Pediatr Res*. 48:725–730.

Guihard-Costa AM, Menez F, Delezoide AL. 2002. Organ weights in human fetuses after formalin fixation: standards by gestational age and body weight. *Pediatr Dev Pathol*. 5:559–578.

Habas PA, Kim K, Corbett-Detig JM, Rousseau F, Glenn OA, Barkovich AJ, Studholme C. 2010a. A spatiotemporal atlas of MR intensity, tissue probability and shape of the fetal brain with application to segmentation. *Neuroimage*. 53:460–470.

Habas PA, Kim K, Rousseau F, Glenn OA, Barkovich AJ, Studholme C. 2010b. Atlas-based segmentation of developing tissues in the human brain with quantitative validation in young fetuses. *Hum Brain Mapp*. 31:1348–1358.

He Y, Chen Z, Evans A. 2008. Structural insights into aberrant topological patterns of large-scale cortical networks in Alzheimer's disease. *J Neurosci*. 28:4756–4766.

Hill J, Dierker D, Neil J, Inder T, Knutsen A, Harwell J, Coalson T, Van Essen D. 2010. A surface-based analysis of hemispheric asymmetries and folding of cerebral cortex in term-born human infants. *J Neurosci*. 30:2268–2276.

Hirota Y, Nakajima K. 2017. Control of neuronal migration and aggregation by Reelin Signaling in the developing cerebral cortex. *Front Cell Dev Biol*. 5:40.

Huang H, Jeon T, Sedmak G, Pletikos M, Vasung L, Xu X, Yarowsky P, Richards LJ, Kostovic I, Sestan N et al. 2013. Coupling diffusion imaging with histological and gene expression analysis to examine the dynamics of cortical areas across the fetal period of human brain development. *Cereb Cortex*. 23:2620–2631.

Huang H, Shu N, Mishra V, Jeon T, Chalak L, Wang ZJ, Rollins N, Gong G, Cheng H, Peng Y et al. 2015. Development of human brain structural networks through infancy and childhood. *Cereb Cortex*. 25:1389–1404.

Huang H, Xue R, Zhang J, Ren T, Richards LJ, Yarowsky P, Miller MI, Mori S. 2009. Anatomical characterization of human fetal brain development with diffusion tensor magnetic resonance imaging. *J Neurosci*. 29:4263–4273.

Johnson MB, Kawasawa YI, Mason CE, Krsnik Z, Coppola G, Bogdanovic D, Geschwind DH, Mane SM, State MW, Sestan N. 2009. Functional and evolutionary insights into human brain development through global transcriptome analysis. *Neuron*. 62:494–509.

Kang HJ, Kawasawa YI, Cheng F, Zhu Y, Xu X, Li M, Sousa AM, Pletikos M, Meyer KA, Sedmak G et al. 2011. Spatio-temporal transcriptome of the human brain. *Nature*. 478:483–489.

Khundrakpam BS, Lewis JD, Reid A, Karama S, Zhao L, Chouinard-Decorte F, Evans AC, Brain Development Cooperative G. 2017. Imaging structural covariance in the development of intelligence. *Neuroimage*. 144:227–240.

Kim H, Lepage C, Maheshwary R, Jeon S, Evans AC, Hess CP, Barkovich AJ, Xu D. 2016. NEOCIVET: towards accurate morphometry of neonatal gyrification and clinical applications in preterm newborns. *Neuroimage*. 138:28–42.

Kim SY, Liu M, Hong SJ, Toga AW, Barkovich AJ, Xu D, Kim H. 2020. Disruption and compensation of Sulcation-based covariance networks in neonatal Brain growth after perinatal injury. *Cereb Cortex*. 30:6238–6253.

Kostovic I, Jovanov-Milosevic N. 2006. The development of cerebral connections during the first 20-45 weeks gestation. *Semin Fetal Neonatal Med*. 11:415–422.

Kostović I, Judaš M, Radoš M, Hrabač P. 2002. Laminar organization of the human fetal cerebrum revealed by histochemical markers and magnetic resonance imaging. *Cereb Cortex*. 12:536–544.

Kostovic I, Vasung L. 2009. Insights from in vitro fetal magnetic resonance imaging of cerebral development. *Semin Perinatol*. 33:220–233.

Kwan KY, Sestan N, Anton ES. 2012. Transcriptional co-regulation of neuronal migration and laminar identity in the neocortex. *Development*. 139:1535–1546.

Lancichinetti A, Fortunato S. 2012. Consensus clustering in complex networks. *Sci Rep*. 2:336.

Lerch JP, Evans AC. 2005. Cortical thickness analysis examined through power analysis and a population simulation. *Neuroimage*. 24:163–173.

Liu M, Lepage C, Jeon S, Flynn T, Kim H, editors. 2019. A Skeleton and Deformation Based Model for Neonatal Pial Surface Reconstruction in Preterm Newborns. In: *2019 IEEE 16th International Symposium on Biomedical Imaging (ISBI)*. Venice, Italy: IEEE.

Lyttelton O, Boucher M, Robbins S, Evans A. 2007. An unbiased iterative group registration template for cortical surface analysis. *Neuroimage*. 34:1535–1544.

Makropoulos A, Robinson EC, Schuh A, Wright R, Fitzgibbon S, Bozek J, Counsell SJ, Steinweg J, Vecchiato K, Passerat-Palmbach J et al. 2018. The developing human connectome project: a minimal processing pipeline for neonatal cortical surface reconstruction. *Neuroimage*. 173:88–112.

Meng Y, Li G, Lin W, Gilmore JH, Shen D. 2015. Cortical surface-based construction of individual structural network with application to early Brain Development study. *Med Image Comput Comput Assist Interv*. 9351:560–568.

Miranda RC. 2012. MicroRNAs and Fetal Brain Development: implications for ethanol teratology during the second trimester period of neurogenesis. *Front Genet*. 3:77.

Newman ME. 2006. Modularity and community structure in networks. *Proc Natl Acad Sci U S A*. 103:8577–8582.

Newman ME, Girvan M. 2004. Finding and evaluating community structure in networks. *Phys Rev E*. 69:026113.

Nie J, Li G, Wang L, Shi F, Lin W, Gilmore JH, Shen D. 2014. Longitudinal development of cortical thickness, folding, and fiber density networks in the first 2 years of life. *Hum Brain Mapp*. 35:3726–3737.

Nosarti C, Mechelli A, Herrera A, Walshe M, Shergill SS, Murray RM, Rifkin L, Allin MP. 2011. Structural covariance in the cortex of very preterm adolescents: a voxel-based morphometry study. *Hum Brain Mapp*. 32:1615–1625.

Rados M, Judas M, Kostovic I. 2006. In vitro MRI of brain development. *Eur J Radiol*. 57:187–198.

Rajagopalan V, Scott J, Habas PA, Kim K, Corbett-Detig J, Rousseau F, Barkovich AJ, Glenn OA, Studholme C. 2011. Local tissue growth patterns underlying normal fetal human brain gyrification quantified in utero. *J Neurosci*. 31:2878–2887.

Rakic P. 1972. Mode of cell migration to the superficial layers of fetal monkey neocortex. *J Comp Neurol*. 145:61–83.

Rakic P. 2003. Developmental and evolutionary adaptations of cortical radial glia. *Cereb Cortex*. 13:541–549.

Robbins S, Evans AC, Collins DL, Whitesides S. 2004. Tuning and comparing spatial normalization methods. *Med Image Anal*. 8:311–323.

Scheinost D, Kwon SH, Lacadie C, Vohr BR, Schneider KC, Papademetris X, Constable RT, Ment LR. 2017. Alterations in anatomical covariance in the prematurely born. *Cereb Cortex*. 27:534–543.

Sidman RL, Rakic P. 1982. Development of the human central nervous system. In: *Histology and Histopathology of the Nervous System*. Springfield: C.C. Thomas.

Sidman RL, Rakic P. 1973. Neuronal migration, with special reference to developing human brain: a review. *Brain Res*. 62:1–35.

Sled JG, Zijdenbos AP, Evans AC. 1998. A nonparametric method for automatic correction of intensity nonuniformity in MRI data. *IEEE Trans Med Imaging*. 17:87–97.

Smart IH, Dehay C, Giroud P, Berland M, Kennedy H. 2002. Unique morphological features of the proliferative zones and postmitotic compartments of the neural epithelium giving rise to striate and extrastriate cortex in the monkey. *Cereb Cortex*. 12:37–53.

Song L, Mishra V, Ouyang M, Peng Q, Slinger M, Liu S, Huang H. 2017. Human Fetal Brain connectome: structural network Development from middle Fetal stage to birth. *Front Neurosci*. 11:561.

Stan AD, Ghose S, Gao XM, Roberts RC, Lewis-Amezcua K, Hatanpaa KJ, Tamminga CA. 2006. Human postmortem tissue: what quality markers matter? *Brain Res*. 1123:1–11.

Takahashi E, Hayashi E, Schmahmann JD, Grant PE. 2014. Development of cerebellar connectivity in human fetal brains revealed by high angular resolution diffusion tractography. *Neuroimage*. 96:326–333.

Thomason ME, Brown JA, Dassanayake MT, Shastri R, Marusak HA, Hernandez-Andrade E, Yeo L, Mody S, Berman S, Hassan SS et al. 2014. Intrinsic functional brain architecture derived from graph theoretical analysis in the human fetus. *PLoS One*. 9:e94423.

Thomason ME, Grove LE, Lozon TA Jr, Vila AM, Ye Y, Nye MJ, Manning JH, Pappas A, Hernandez-Andrade E, Yeo L et al. 2015. Age-related increases in long-range connectivity in fetal functional neural connectivity networks in utero. *Dev Cogn Neurosci*. 11:96–104.

Tymofiyeva O, Hess CP, Ziv E, Lee PN, Glass HC, Ferriero DM, Barkovich AJ, Xu D. 2013. A DTI-based template-free cortical connectome study of brain maturation. *PLoS One*. 8:e63310.

Tymofiyeva O, Hess CP, Ziv E, Tian N, Bonifacio SL, McQuillen PS, Ferriero DM, Barkovich AJ, Xu D. 2012. Towards the "baby connectome": mapping the structural connectivity of the newborn brain. *PLoS One*. 7:e31029.

van den Heuvel MP, Kersbergen KJ, de Reus MA, Keunen K, Kahn RS, Groenendaal F, de Vries LS, Benders MJ. 2015. The neonatal connectome during preterm Brain Development. *Cereb Cortex*. 25:3000–3013.

Vasung L, Lepage C, Rados M, Pletikos M, Goldman JS, Richiardi J, Raguz M, Fischi-Gomez E, Karama S, Huppi PS et al. 2016. Quantitative and qualitative analysis of transient Fetal compartments during prenatal human Brain Development. *Front Neuroanat*. 10:11.

Wang HZ, Suh JW, Das SR, Pluta JB, Craige C, Yushkevich PA. 2013. Multi-atlas segmentation with joint label fusion. *Ieee T Pattern Anal*. 35:611–623.

Webb SJ, Monk CS, Nelson CA. 2001. Mechanisms of postnatal neurobiological development: implications for human development. *Dev Neuropsychol*. 19:147–171.

Winkler AM, Sabuncu MR, Yeo BT, Fischl B, Greve DN, Kochunov P, Nichols TE, Blangero J, Glahn DC. 2012. Measuring and comparing brain cortical surface area and other areal quantities. *Neuroimage*. 61:1428–1443.

Xia J, Wang F, Benkarim OM, Sanroma G, Piella G, Gonzalez Ballester MA, Hahner N, Eixarch E, Zhang C, Shen D et al. 2019. Fetal cortical surface atlas parcellation based on growth patterns. *Hum Brain Mapp*. 40:3881–3899.

Yap PT, Fan Y, Chen Y, Gilmore JH, Lin W, Shen D. 2011. Development trends of white matter connectivity in the first years of life. *PLoS One*. 6:e24678.

Zhan J, Dinov ID, Li J, Zhang Z, Hobel S, Shi Y, Lin X, Zamanyan A, Feng L, Teng G et al. 2013. Spatial-temporal atlas of human fetal brain development during the early second trimester. *Neuroimage*. 82:115–126.

Zhang Z, Hou Z, Lin X, Teng G, Meng H, Zang F, Fang F, Liu S. 2013. Development of the fetal cerebral cortex in the second trimester: assessment with 7T postmortem MR imaging. *Am J Neuroradiol*. 34:1462–1467.

Zhang Z, Liu S, Lin X, Teng G, Yu T, Fang F, Zang F. 2011. Development of laminar organization of the fetal cerebrum at 3.0T and 7.0T: a postmortem MRI study. *Neuroradiology*. 53:177–184.

Zhao T, Mishra V, Jeon T, Ouyang M, Peng Q, Chalak L, Wisnowski JL, Heyne R, Rollins N, Shu N et al. 2019. Structural network maturation of the preterm human brain. *Neuroimage*. 185:699–710.

Zielinski BA, Gennatas ED, Zhou J, Seeley WW. 2010. Network-level structural covariance in the developing brain. *Proc Natl Acad Sci U S A*. 107:18191–18196.